International Journal on Magnetic Particle Imaging
Vol 10, No 1, Suppl 1, Article ID 2403014, 5 Pages

Infinite Science Publishing

Proceedings Article

Multicontrasting MPS by dual-tone nonlinearity probing

T. I. Bikulov[a,b,*] · F. Eivazi[a,b] · A. Offenhäusser[a,b] · H.-J. Krause[a]

[a]Institute of Biological Information Processing, Forschungszentrum Jülich, 52425 Jülich, Germany
[a]Faculty of Mathematics, Computer Sci. and Natural Sci., RWTH Aachen, 52056 Aachen, Germany
[*]Corresponding author, email: timur.bikulov@rwth-aachen.de

Abstract

Novel MPI-based modalities such as multi-contrast imaging or remote viscosity recording require independent measurement of at least two or more magnetic particle types simultaneously. Particle response models based on the Fokker-Plank equation allow independent reconstruction of core and hydrodynamic diameters. However, due to complexity and stochastic character, they remain a black box for explaining the origin of measured nonlinear distortions. A model is required to suggest which frequency lines to measure, which fields to apply for reconstruction of particle core size distribution, and to explicitly show limitations of setup and measurement scheme (e.g., the range of core diameters available for reconstruction). Assuming that the amplitude of the sample magnetic moment and its distortions are determined by the number of excited magnetic moments, and response phase is governed by amplitude-dependent relaxation mechanisms, we show how and under what conditions two-tone systems become the key to independent measurement of the response from particles of different diameters.

I. Introduction

Novel MPI-based modalities such as multi-contrast tomography [1] , remote measurement of temperature [2] and viscosity [3] show great potential. They are based on phase response measurement of magnetic nanoparticles (MNP). However, measuring only the phase of a mixture of more than two contrast agents alone will not distinguish their contributions. Moreover, remote viscosity/temperature measurement also requires at least two degrees of freedom because viscosity and temperature affect the phase simultaneously. The MNP nonlinear response features can be potentially used to separate the responses from different MNP types [4]. There is a great variety of models describing the different aspects of nonlinear and dynamic MNP response. Phenomenological linear lumped parameter models of integer [5] and fractional [6] orders describe ac susceptometry of MNP colloids. Volterra series [7] provide a phenomenological description for MNP nonlinear response, mostly used as a numerical response model in quasi-static approximation [8]. Statistical physics models based on the Langevin equation [9] and the Fokker-Planck equation [10] describe thermal fluctuations and relaxation mechanisms in magnetic colloids, respectively. They can be used to numerically obtain both amplitude and phase of MNP response. In contrast to numerical modelling, we treat MNP as a passive mixer (or modulator) that modulates both amplitude and phase. Following the approach from [11], we exploit the Bessel function apparatus and introduce a Hilbert transform-based model to interconnect Intermodulation harmonics (IM) in form of Fourier coefficients $A_{k_1\omega_1+k_2\omega_2}$ of measured magnetization $m(h)$ at frequency $k_1\omega_1 + k_2\omega_2$,

$$A_{k_1\omega_1+k_2\omega_2} = \int_{-\infty}^{\infty} m(h(t))\exp(-\mathrm{i}t(k_1\omega_1 + k_2\omega_2))\,\mathrm{d}t \quad (1)$$

10.18416/ijmpi.2024.2403014

with MNP sample properties determined by its core diameter d_c and its relaxation properties. By postulating that the real MNP sample can be described as a superposition of multiple passive mixers, we apply this model to reconstruct joint distribution of core diameters and corresponding phases due to relaxation from the experimental data.

II. Dynamic nonlinear particle response

Let us consider an ensemble of MNP that weakly interact $\left(\mu_0 m_0^2 / r_0^3 \ll k_B T\right)$ where m_0 is particle average magnetic moment and $r_0 = d_c + 2t_s$ where t_s is a nonmagnetic shell thickness. In such a mode, we can assume that this system has no memory but rate-dependent hysteresis is present due to relaxation. We introduce immediate sample magnetization $m(h)$ that depends on immediate field value h

$$m(h) = m_g(h) \cdot \beta(h) \cdot \exp\left(\mathrm{i} \cdot \theta_f(h)\right) \tag{2}$$

as an independent product of amplitude (AM) $m_g(h) \cdot \beta(h)$ and phase (PM) $\theta_f(h)$ modulations. We define our model (1) in terms of Hilbert transform that permits arbitrary shape of the excitation signal $h(t)$ and is suitable for modulated signal analysis. Based on Langevin theory of paramagnetic gas, we assume that AM is related to modulation of the number of instantaneously excited magnetic moments whereas PM represents relaxation processes. AM is represented by a product of a nonlinear part, $m_g(h)$, that is responsible for nonlinear properties of the magnetization curve, and a linear sub-term $\beta(h)$ responsible for rate-dependent losses. Maximum magnetization for polydisperse colloid is achieved experimentally only in static measurement, when rate-dependent losses are absent. That is why we presume the $m_g(h)$ to be equal to the static magnetization curve of the sample [15],

$$m_g(h) = N_p \int_0^\infty \frac{\pi M_s}{6} x^3 \mathscr{L}\left(h x^3 \frac{\pi M_s}{6 k_B T}\right) \rho_c(x) \mathrm{d}x \tag{3}$$

where $\mathscr{L}(x) = \coth(x) - 1/x$ is Langevin curve, M_s is saturation magnetization ($M_s = 476$ kA/m for magnetite), $k_B T$ is thermal energy ($T = 298$ K), $\rho_c(x)$ is the probability density function (PDF) of the MNP core diameter distribution, and N_p is the total number of particles.

According to ac susceptometry experiments, the phase term of typical MNP sample remains in $\theta_f(h) \in [0°, 90°)$ range and response amplitude drops down for higher field rates. That is why we approximate dynamic particle response with first order (Debye) system [12] through its effective relaxation time $\tau_{\mathrm{eff}}(h)$ and instantaneous frequency $\omega_h(h)$,

$$\beta(h) = \frac{1}{\sqrt{1 + \left(\langle|\omega_h(h)|\rangle \, \tau_{\mathrm{eff}}(h)\right)^2}} \tag{4}$$

$$\theta_f(h) = \arctan\left(\langle|\omega_h(h)|\rangle \, \tau_{\mathrm{eff}}(h)\right) \tag{5}$$

$$\langle x(t)\rangle = \frac{1}{T_p} \int_0^{T_p} x(t) \mathrm{d}t. \tag{6}$$

$\langle|\omega_h(h)|\rangle$ is the averaged absolute value of the instantaneous frequency $\omega_h(t)$ over the period T_p of excitation signal $h(t) = h\left(t + T_p\right)$,

$$\omega_h(t) = \frac{\mathrm{d}}{\mathrm{d}t} \arctan\left(\frac{\mathscr{H}(h(t))}{h(t)}\right) \tag{7}$$

where $\mathscr{H}(\cdot)$ is Hilbert transform. Note that $m_g(h)$ depends on absolute value of h whereas $\beta(h)$ and $\theta_f(h)$ are rate-dependent, so using the instantaneous frequency (7) and phase (5), we obtain equivalent excitation parameters for the system response as in single tone measurement. The model (2) fulfils the two extreme cases of static measurement of magnetization curve,

$$\lim_{\omega \to 0} m(H \cdot \cos(\omega t)) = m_g(H), \tag{8}$$

and susceptometry measurement with ac field,

$$\lim_{\varepsilon \to 0} m(\varepsilon \cdot \cos(\omega t)) \propto \varepsilon e^{\mathrm{i} \cdot \arctan(-\omega \tau_{\mathrm{eff}})} / \sqrt{1 + (\omega \tau_{\mathrm{eff}})^2}. \tag{9}$$

Without loss of generality, this model can be extended to a fractional order model that better reflects the susceptometry behavior of real MNP colloids [12].

III. Analytical response in dual-tone case

Let the excitation field $h(t)$ consist of two harmonic tones,

$$h(t) = H_1 \cos(\omega_1 t) + H_2 \cos\left(\omega_2 t + \Delta\varphi\right) \tag{10}$$

that fulfil the relations,

$$\begin{cases} H_2 > H_1 \\ \omega_1 = k\omega_2, k \in \mathbb{Z}^+, \omega_2 = 2\pi / T_p \\ \omega_1 H_1 \gg \omega_2 H_2 \end{cases}. \tag{11}$$

PDF $\rho_e(h)$ of (10) under conditions (11) is close to arcsin-type PDF $\rho_e(h')$ of single harmonic excitation at low-frequency (LF) $h'(t) = H_2 \cos\left(\omega_2 t + \Delta\varphi\right)$,

$$\rho_e(h) \approx \rho_e\left(h'\right) = 1 / \left(\pi \sqrt{H_2^2 - h'^2}\right). \tag{12}$$

In our case ($\omega_1 = 40.5$ kHz $\cdot 2\pi$, $\omega_2 = 10$ Hz $\cdot 2\pi$), $h(t)$ remains 90% of T_p period in range $|h| \in [0.76 \cdot H_2, H_2]$, so behavior of $m(h)$ in this range determines Fourier components $A_{k_1\omega_1 + k_2\omega_2}$ by 90%.

Shimbo [13] used Bessel functions to describe the IM products $A_{k_1\omega_1 + k_2\omega_2 + \ldots + k_n\omega_n}$ in a passive non-linear

device with immediate transfer function m(h) being exposed to n harmonic tones ω_i of amplitudes H_i ($i = 1 \dots n$),

$$A_{k_1\omega_1+k_2\omega_2+\cdots+k_n\omega_n}(H_1, H_2, \cdots, H_n) = \int_0^\infty r \prod_{l=1}^{n} J_{k_l}(H_l r) \int_0^\infty \rho\, m(\rho) \cdot J_1(r\rho)\, \mathrm{d}\rho\, \mathrm{d}r \qquad (13)$$

where $J_k(x)$ are Bessel functions of first kind of order k. This expression is a generating function for the series that we have suggested earlier [4]. Imboldi [14] has shown for the case of two tone excitation (10) and constancy of PM modulation ($\theta_f(h) = \theta_f$) (13) simplifies to,

$$A_{k_1\omega_1+k_2\omega_2} = \frac{2}{\pi} \int_0^\infty \hat{F}(f_h) \cdot J_{k_1}(H_1 f_h) \cdot J_{k_2}(H_2 f_h)\, \mathrm{d}f_h \qquad (14)$$

where $\hat{F}(f_h)$ is a Fourier transform of $m(h)$ in field space. Maass provides the Fourier transform of the Langevin curve [11],

$$\widehat{\mathscr{L}}(f_h) = -i \frac{f_h}{|f_h|} \frac{2\pi e^{-\pi|f_h|}}{1 - e^{-\pi|f_h|}}, |f_h| \neq 0. \qquad (15)$$

Substitution of (14) into $\hat{F}(f_h)$ in (13) and application of Fourier transform scaling property,

$$\mathscr{L}(\alpha_p x) \leftrightarrow \frac{1}{|\alpha_p|} \widehat{\mathscr{L}}\left(\frac{f_h}{\alpha_p}\right), \; \alpha_p = \frac{\pi M_s d_c^3}{6 k_B T}, \qquad (16)$$

provides a response for a monodisperse MNP sample $A_{k_1\omega_1+k_2\omega_2}(H_2, d_c)$ as a function of LF-field amplitude H_2 and core diameter d_c.

In case $k_1 = 1 \wedge k_2 = 2n$, $n \in \mathbb{Z} \setminus \{0\}$, $A_{k_1\omega_1+k_2\omega_2}(H_2, d_c)$ vanishes for $H_2 \to 0$ and for $H_2 \to \infty$, forming a bell-shaped curve (Fig. 1). The curve has its maximum when $h(t)$ remains predominantly in nonlinear region of $m(h)$, in the vicinity of second derivative extremum $H_c \propto d_c^{-3}$,

$$\underset{h}{\operatorname{argmax}} \left| \frac{\mathrm{d}^2 m_g(h)}{\mathrm{d}h^2} \right| = H_c. \qquad (17)$$

The field dependence of effective relaxation time $\tau_{\mathrm{eff}}(h)$ directly follows from the original derivations made by Brown [17] and Néel [16]. Due to limited range of H_2 where $A_{k_1\omega_1+k_2\omega_2}(H_2, d_c)$ is non-zero, the field dependence of relaxation time for the case of excitation field (10) under conditions (11) can be avoided and approximated with constant $\tau_{\mathrm{eff}} \approx \tau_{\mathrm{eff}}(H_c)$, meaning constancy of PM.

IV. Experimental reconstruction

To reconstruct the joint core diameter-phase distribution $\rho(d_c, \theta_f)$ in form of a histogram vector $\mathrm{h_b}$ with $\mathrm{h_{b}}_i \in \mathbb{C}$ (where $i = 1, \dots, N_m$, $N_m = 40$),

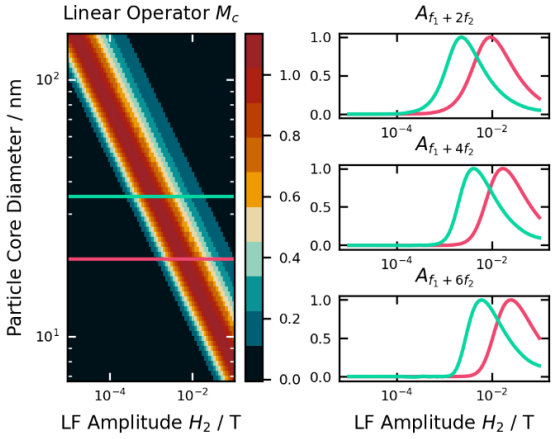

Figure 1: Left: Linear operator M_c that maps visible diameter bins d_c to normalized $A_{\omega_1+2\omega_2}$ amplitudes. Right: Normalized amplitude $A_{\omega_1+k_2\omega_2}(H_2, d_c)$ for $k_2 \in \{2, 4, 6\}$ and $d_c \in \{20, 35\}$ nm in red and green, respectively.

which corresponds to core diameters vector $\mathrm{d_c} = (x_i \in \mathbb{R} \mid x_i = s_l(d_{min}, d_{max}, i, N_m),\ d_{min} \leq x \leq d_{max})$,

$$s_l(x, y, i, n) = \sqrt[n]{x^{n-i} y^i}, \qquad (18)$$

N_m synchronous demodulation measurements $\mathrm{b_m}_i \in \mathbb{C}$ of $A_{\omega_1+2\omega_2}$ IM are conducted. $H_1 = 0.5\ \mathrm{mT}/\mu_0$ amplitude remains constant. LF field H_2 is varied in log-scale range $[H_1, H_{max}]$, $\mathrm{H}_{2i} = s_l(H_1, H_{max}, i, N_m)$, where $H_{max} = 20\ \mathrm{mT}/\mu_0$ is the maximum available LF-amplitude. In double log-scaling, the dependence $H_c \propto d_c^{-3}$ becomes linear and the information about the core diameter distribution is uniformly spread along the measurement range. Range $[d_{min}, d_{max}]$ of reconstructable MNP core diameters is selected using (14-16),

$$\begin{cases} d_{min} = \operatorname{argmax}_x A_{\omega_1+2\omega_2}(H_{max}, x) \\ d_{max} = \operatorname{argmax}_x A_{\omega_1+2\omega_2}(H_1, x) \end{cases}, x \in \mathbb{R}^+ \qquad (19)$$

The real-valued $N_m \times N_m$ measurement matrix M_c is formed (Fig.1, left) according to,

$$[M_c]_{i,j} = A_{\omega_1+2\omega_2}(\mathbf{H_2}_j, \mathbf{d_c}_i)/F_i \qquad (20)$$

where F_i is a normalization factor that accounts for α_p^{-1}amplitude scaling according to (16),

$$F_i = \max_x \left| A_{\omega_1+2\omega_2}(x, \mathbf{d_c}_i) \right|, x \in \mathbb{R}^+ \qquad (21)$$

Phase origin of the demodulation is selected and fixed once for all measurements so that $\mathrm{Re}\{\mathrm{b_m}_i\}$, $\mathrm{Im}\{\mathrm{b_m}_i\} \geq 0$. $\mathrm{b_m}$is obtained by subtracting the background measurement $\mathrm{b_{bg}}$ (w/o sample) from the raw measurement (w/ sample) $\mathrm{b_r}$,

$$\mathbf{b_m} = \mathbf{b_r} - \mathbf{b_{bg}}. \qquad (22)$$

The SNR of the measurement is calculated using,

$$\mathrm{SNR} = 20 \cdot \lg\left(\|\mathbf{b_r}\|_\infty / \left\|\mathbf{b_{bg}}\right\|_\infty\right) \tag{23}$$

The reconstruction of $\mathrm{h_b}$ is conducted by solving Tikhonov-regularized linear inverse problem using non-negative least-squares algorithm constraining $\mathrm{Re}\{\mathrm{h_b}_i\}$, $\mathrm{Im}\{\mathrm{h_b}_i\} \geq 0$,

$$\begin{bmatrix} M_c \\ \lambda E \end{bmatrix} \mathbf{h_b} = \begin{bmatrix} \mathbf{b_m} \\ \mathbf{0}_{N_m,1} \end{bmatrix} \tag{24}$$

where E is a unity matrix and $\lambda = 0.1$ is a Tikhonov regularization parameter. The amplitudes of the histogram bins $\left|\mathrm{h_b}_i\right|$ correspond to the number of contributing particles (AM) of a specific core size $\mathrm{d_c}_i$. Complex arguments $\arg\left(\mathrm{h_b}_i\right)$ correspond to resulting effective phase θ_{f_i} of a $\mathrm{d_c}_i$. fraction due to relaxation (PM). To demonstrate mutual independence of AM and PM, we conduct an experiment in which the hydrodynamic diameter (hence only PM properties) is sequentially increased.

V. MNP with varying hydrodynamic diameter

We employed commercial superparamagnetic streptavidinated MNP (Synomag®-D, 70 nm from Micromod, Rostock, Germany). We diluted the particles with 1 mM PBS (Phosphate-Buffered Saline) to reach to a final concentration of 0.25 mg/ml within a sample volume of 130 µl. This resulting sample (Syn70Orig) was measured.

In order to increase the hydrodynamic size of the particles, we incubated the sample with CRP Monoclonal Antibody (C7) antibodies conjugated with Biotin (ThermoFisher, USA). Likewise, the antibodies were diluted with PBS to reach a concentration of 0.1 mg/ml. Subsequently, the particles were incubated with 10 µl of antibodies for a duration of 20 min. The resulting sample (Syn70Ab) of particles with antibodies was measured to explore the increase in hydrodynamic size.

Subsequently, we added C-reactive protein (CRP) from Merck KGaA, Germany, diluted to a concentration of 0.05 mg/ml, in order to further enhance the hydrodynamic size of the particles. We added 10 µl of CRP to sample Syn70Ab and incubated it for 90 min. The resulting sample (Syn70AbAg) with a volume of 150 µl was measured.

VI. Results and discussion

Fig. 1 shows a linear mapping between particle core diameter and LF-field scan for dual-tone excitation. Particles of different core diameters (red and green lines, Fig.1 left and right) have peak amplitudes for distinct H_2 amplitudes forming a quasi-orthogonal space limited by the aperture of the bell-shaped curve that can be used for independent read-out in multicontrast systems. Note that according to expression (14) in single-tone excitation case, the amplitude scan gives a step-like curve that does not allow this approach. From numerical evaluation of (14) (Fig.1 right), it follows that measurement of higher order IM reduces the bell-shaped curve width on LF-scan increasing d_c-resolution. Also, it expands the upper range of visible diameters d_{max}. At the same time, it puts higher demands on LF field amplitude and is limited by the noise floor. Measurement of several IM at a time allows simultaneous probing multiple diameters.

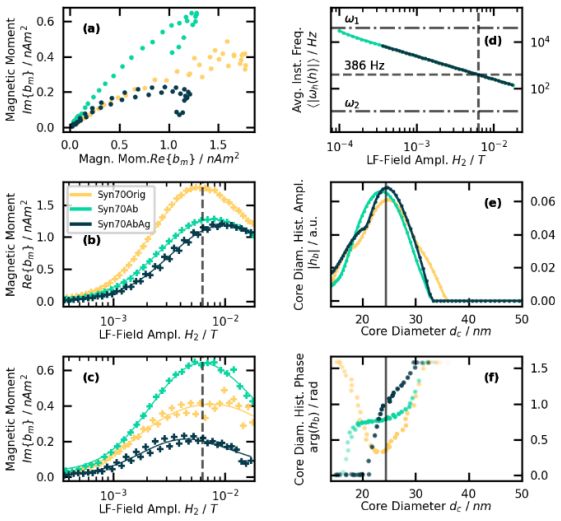

Figure 2: Reconstruction of the phase – core diameter distribution of the samples. (a) – IM measured response of $A_{\omega_1+2\omega_2}$ in the complex plane. (b), (c)- Real and imaginary part of $A_{\omega_1+2\omega_2}$ components (scatter) and model fit (solid) (d)- Averaged instantaneous frequency $\langle|\omega_h(h)|\rangle$ dependency of LF-amplitude H_2 (e) – Absolute values of reconstructed histogram vector components $\mathbf{h_b}$ (f) – Joint phase – core diameter distribution

Fig. 2 shows the experimental results of phase-core diameter distribution reconstruction $\mathrm{h_b}$ for three samples (Syn70Orig, Syn70Ab, Syn70AbAg) of increasing hydrodynamic diameters. The measured $\mathrm{b_m}$ vectors are depicted in Fig. 2 a, exhibiting a hook-shape. Real and imaginary projections are plotted vs actual LF field amplitude in Fig. 2 b,c. No clear pattern is recognized at this stage. SNR (23) was >6.9 dB for all experiments. The reconstruction procedure described in section IV was applied to the data and corresponding vectors $\mathrm{h_b}$ were obtained (Fig. 2 e,f). The model (2,14-16) resulted in a good agreement (MAE < 29.5 pAm^2, $N_m = 40$) with the experimental data (Fig. 2 (b,c)). The resulting amplitude $\left|\mathrm{h_b}_i\right|$ of core diameter histogram (Fig. 2 (e)) remains invariant for all three cases. At the same time, phase portrait $\arg\left(\mathrm{h_b}_i\right)$ on the joint phase-core diameter distribution changes

10.18416/ijmpi.2024.2403014

(Fig. 2, f), demonstrating independence of AM and PM in the MNP sample. The change can be interpreted using average instant frequency curve (Fig. 2 (d)) calculated using (6-7) for corresponding H_2 values. Peaks on LF-scan (Fig. 2 b,c) correspond to core diameter of ∼24.4 nm (Fig .1) and average instant frequency of ∼386 Hz. Physical interpretation of instantaneous frequency in this context can be reformulated as an average number of sign changes of excitation field per period. In dual-tone measurement mode under (11) conditions smaller core diameters correspond to larger LF-field amplitudes and to smaller instantaneous frequencies.

VII. Conclusions

Using the analytical expressions (14)-(16) for intermodulation product $A_{k_1\omega_1+k_2\omega_2}$, we showed that at least two tones of excitation field are needed to implement nonlinearity-based multi-contrast MPS system. Due to asymptotic vanishing of LF-scan, dual tone excitation readout scheme under conditions (11) also permits waiving field dependence of the effective relaxation time $\tau_{\text{eff}} \approx \tau_{\text{eff}}(H_c)$, allowing to model the MNP sample as a superposition of passive mixers with constant phases. Passive mixer model (2) enabled us to explain the hook-shape of the LF-scan complex response as a superposition of MNPs with joint core size $|\mathrm{h}_{\mathrm{b}_i}|$ and phase $\arg(\mathrm{h}_{\mathrm{b}_i})$ distribution. We proposed an optimal measurement scheme for nonlinearity-based multicontrast MPS, explained the limits of this approach and advantages of simultaneous measurement of multiple IMs. We applied the scheme in experiment to demonstrate independence of AM and PM in MNP sample with varying hydrodynamic diameter. The experiment shows that the reconstructed distribution allows independent determination of the particle core size distribution in the absolute values of $|\mathrm{h}_{\mathrm{b}_i}|$ and the hydrodynamic size changes in its complex phase $\arg(\mathrm{h}_{\mathrm{b}_i})$.

Acknowledgments

Research funding from German Federal Ministry of Food and Agriculture (BMEL), contract 2818710C19, and from Deutsche Forschungsgemeinschaft (DFG), grant 445454801, is gratefully acknowledged.

Author's statement

Conflict of interest: Authors state no conflict of interest.

References

[1] C. Shasha, *Discriminating nanoparticle core size using multi-contrast MPI*, Phys. Med. Biol., vol. 64-7, 074001, Mar. 2019.
[2] I. M. Perreard, *Temperature of the magnetic nanoparticle microenvironment: Estimation from relaxation times*, Phys. Med. Biol., vol. 59-5, pp. 1109-1119, Feb. 2014.

[3] M. Möddel, *Viscosity quantification using multi-contrast magnetic particle imaging*, New J. Phys. vol. 20-8, 083001, Aug. 2018.

[4] T. Bikulov, *Passive mixer model for multi-contrast magnetic particle spectroscopy*, Int J Magn Part Imag, vol 9-1, 2303087, Mar 2023

[5] L. Tu, *Real-time measurement of Brownian relaxation of magnetic nanoparticles by a mixing-frequency method*, Appl. Phys. Lett., vol. 98-21,213702, May 2011.

[6] T. Yoshida, *Simulation and quantitative clarification of AC susceptibility of magnetic fluid in nonlinear Brownian relaxation region*, Jpn. J. Appl. Phys., vol. 48-12, 127002, Dec. 2009.

[7] B. W. Ficko, *Nonlinear Spectroscopic Characterization and Volterra Series Inspired Modeling of Magnetic Nanoparticles*, IEEE Trans. Magn., vol. 53-2, pp. 1–12, Feb. 2017.

[8] H. -J. Krause, *Magnetic particle detection by frequency mixing for immunoassay applications*, J. Magn. Magn. Mater., vol. 311-1, pp. 436–444, Dec. 2007.

[9] W. F. Brown, *Thermal Fluctuations of a Single-Domain Particle*, Phys. Rev., vol. 130-5, pp. 1677–1686, Jun. 1963.

[10] J. Weizenecker, *The Fokker–Planck equation for coupled Brown–Néel-rotation*, Phys. Med. Biol., vol. 63-3, 035004, Jan. 2018.

[11] M. Maass, *Representation of Magnetic Particle Imaging in Fourier Space*, Int. J. Magn. Part. Imaging, vol. 6-1, pp. 1–21, Dec. 2019.

[12] P. C. Fannin, *The measurement of the frequency dependent susceptibility of magnetic colloids*, J. Magn. Magn. Mater., vol. 72-1, pp. 95–108, Mar. 1988.

[13] O. Shimbo, *Effects of intermodulation, AM-PM conversion, and additive noise in multicarrier TWT systems*, Proc. IEEE, vol. 59-2, pp. 230–238, Feb. 1971.

[14] E. Imboldi, *AM-to-PM conversion and intermodulation in nonlinear devices*, Proc. IEEE, vol. 61-6, pp. 796–797, Jun. 1973.

[15] U. M. Engelmann, *Comparative Modeling of Frequency Mixing Measurements of Magnetic Nanoparticles Using Micromagnetic Simulations and Langevin Theory*, MDPI Nanomat., vol.11, pp. 1257, Mar. 2021.

[16] L. Néel, *Some theoretical aspects of rock-magnetism*, Adv. Phys., vol. 4-14, pp. 191-243, Apr. 1955.

[17] W.F., Jr. Brown, *Thermal Fluctuations of Fine Ferromagnetic Particles*, IEEE T. Magn., vol. 15-5, pp. 1196-1208, Jan. 1979.

[18] R.E. Rosensweig, *Ferrohydrodynamics*. Mineola, NY: Dover Publications, 1985.

